Mon. Not. R. Astron. Soc. **000**, 1–?? (0000) Printed 16 August 2018 (MN LATEX style file v2.2)

# The effect of Lyman $\alpha$ radiation on mini-Neptune atmospheres around M stars: application to GJ 436b

Yamila Miguel[1⋆], Lisa Kaltenegger[1,2], Jeffrey L. Linsky[3] and Sarah Rugheimer[2]
[1] *Max Planck Institut für Astronomie, Königstuhl 17, 69117, Heidelberg, Germany*
[2] *Harvard Smithsonian Center for Astrophysics, 60 Garden St., Cambridge, MA, 02138 USA*
[3] *JILA, University of Colorado and NIST, 440 UCB Boulder, CO 80309-0440, USA*

16 August 2018

arXiv:1410.2112v1 [astro-ph.EP] 8 Oct 2014

**ABSTRACT**

Mini-Neptunes orbiting M stars are a growing population of known exoplanets. Some of them are located very close to their host star, receiving large amounts of UV radiation. Many M stars emit strong chromospheric emission in the H I Lyman $\alpha$ line (Ly$\alpha$) at 1215.67 Å, the brightest far-UV emission line. We show that the effect of incoming Ly$\alpha$ flux can significantly change the photochemistry of mini-Neptunes' atmospheres. We use GJ 436b as an example, considering different metallicities for its atmospheric composition. For solar composition, $H_2O$-mixing ratios show the largest change because of Ly$\alpha$ radiation. $H_2O$ absorbs most of this radiation, thereby shielding $CH_4$, whose dissociation is driven mainly by radiation at other far-UV wavelengths ($\sim$ 1300 Å). $H_2O$ photolysis also affects other species in the atmosphere, including H, $H_2$, $CO_2$, CO, OH and O. For an atmosphere with high metallicity, $H_2O$- and $CO_2$-mixing ratios show the biggest change, thereby shielding $CH_4$. Direct measurements of the UV flux of the host stars are important for understanding the photochemistry in exoplanets' atmospheres. This is crucial, especially in the region between 1 and $10^{-6}$ bars, which is the part of the atmosphere that generates most of the observable spectral features.

**Key words:** planets and satellites: general - planets and satellites: atmospheres

## 1 INTRODUCTION

Recent exoplanet surveys have discovered the first planets with sizes between 2 Earth radii ($R_{\rm Earth}$) and $3.5R_{\rm Earth}$, the size of Neptune. These planets, known as mini-Neptunes, revolve around the M stars GJ 436b (Butler et al. 2004), GJ 1214b (Charbonneau et al. 2009), Kepler 26b and Kepler 32d (Borucki et al. 2011) and GJ 3470b (Bonfils et al. 2012). Since mini-Neptunes around M stars are expected to be abundant (Laughlin et al. 2004) and M stars are the most common stars in the solar neighborhood (Chabrier 2003), we expect that many more mini-Neptunes will be discovered in the near future.

Since M stars have low effective temperatures, the bulk of their flux is emitted in the optical and near IR. Inactive M stars have very low-photospheric–UV-continuum emission when compared to solar-type stars. Direct observations of active M dwarfs show a high flux in the far-UV (FUV 912–1700 Å) (Shkolnik & Barman 2014), and the percentage of total UV flux from the star in the H I Lyman $\alpha$ line (Ly$\alpha$) is between 37 and 75 per cent compared to 0.04 per cent for the Sun (France et al. 2013). While most of the stellar Ly$\alpha$ radiation is scattered or absorbed in the interstellar medium, Ly$\alpha$ is the brightest FUV emission line in the stellar spectrum seen by an exoplanet (France et al. 2013) which makes this emission line critical for atmospheric photochemistry.

While the effect of extreme-UV irradiation (EUV 200–911 Å) was studied for Earth-like (Lammer et al. 2011) and giant planets (Yelle 2004; Lammer et al. 2003; Lecavelier des Etangs et al. 2004; Yelle 2006; Murray-Clay et al. 2009; Koskinen et al. 2010; Sanz-Forcada et al. 2011; Lecavelier des Etangs et al. 2012) and the consequence of high FUV M star irradiation was explored for habitable planets' atmospheres (Scalo et al. 2007; Buccino et al. 2007; Segura et al. 2010), the effect of FUV irradiation and especially Ly$\alpha$ flux on hot mini-Neptune atmospheres has not yet been evaluated. Solar Ly$\alpha$ radiation is known to have a strong impact on the photochemistry of the planets in our Solar System, and the effects of stellar Ly$\alpha$ radiation on the photochemistry of hot extrasolar planets are expected to be important, but such effects have not yet been quantified. In particular, the effect of Lyman-$\alpha$ radiation on the thermal profile in

⋆ miguel@mpia.de

mini-Neptune atmospheres is only beginning to be studied (Lavvas et al. 2011).

We have performed 1D simulations of hot mini-Neptune atmospheres under different irradiation conditions to make a deeper exploration of the effects of Ly$\alpha$ flux on the photochemistry. We focus here on the mini-Neptune GJ 436b as an example, using recent UV observations including the reconstructed Ly$\alpha$ flux (France et al. 2013).

## 2 MODEL DESCRIPTION

### 2.1 Stellar flux

GJ 436 is an M3 dwarf ($T_{eff,\star}$ = 3416 K) with a radius $R_\star = 0.455 R_\odot$ (von Braun et al. 2012). Its coronal flux ($\log L_X = 27.16 \pm 0.34$) is smaller than the mean for M dwarfs ($\log L_X = 27.6$), indicating a low activity corona for GJ 436 (Poppenhaeger et al. 2010). The first reconstructed Ly$\alpha$ emission line profile performed for GJ 436 was based on (HST/STIS) observations (Ehrenreich et al. 2011). Here we use the most recent UV spectral observation of GJ 436 from 1150 to 3140 Å (France et al. 2013), including the reconstructed stellar Ly$\alpha$ emission line profile, which is 1750 ergs cm$^{-2}$ s$^{-1}$ at 0.03AU (France et al. 2013; Linsky et al. 2013). The spectrum is available in the MUSCLES (Measurements of the Ultraviolet Spectral Characteristics of Low-mass Exoplanetary Systems) website[1]. We merged those UV observations with optical synthetic spectra between 2800 and 45450 Å from the PHOENIX models (Allard et al. 2007). We adopt [Fe/H]=0.04 (Rojas-Ayala et al. 2012), $Vsin(i) < 1$ km s$^{-1}$ (Marcy & Chen 1992) and Log(g)=4.83 (Maness et al. 2007).

The resulting GJ 436 flux for $\lambda < 8550$ Å is shown in Fig. 1(a) (grey solid), with the black line showing the binned-stellar input used in our code at a resolution of 2 Å in the FUV and 16 to 50 Å from 2100 to 45450 Å. Note that we use the stellar flux between 1200 and 8550 Å in our photochemical calculations. To analyze the importance of the Ly$\alpha$ flux in exoplanet atmospheres, we model 4 scenarios shown in Fig. 1(b): GJ 436b as irradiated by a star with 1000 x Ly$\alpha$ (green), 100 x Ly$\alpha$ (blue), 10 x Ly$\alpha$ (orange), and 1 x Ly$\alpha$ (black), where n x Ly$\alpha$ is the reconstructed Ly$\alpha$ flux for GJ 436 multiplied by the factor n. Since Ly$\alpha$ radiation could be absorbed by an exoplanet's upper atmosphere (Lavvas et al. 2011), we also explore three scenarios where Ly$\alpha$ flux is reduced to 0.1 x Ly$\alpha$ (red), 0.01 x Ly$\alpha$ (blue) and 0.001 x Ly$\alpha$ (green line), as shown in Fig. 1(c). Note that all M dwarf stars have chromospheres with a wide range of activity, and our calculations explore the effects of extreme differences in Ly$\alpha$ fluxes on exoplanet atmospheres. One thousand times the Ly$\alpha$ flux of GJ 436 corresponds to a very active M dwarf star, and 0.001 x Ly$\alpha$ corresponds to very strong absorption of that radiation in the planet's extended upper atmosphere. We have not considered variations in the total FUV flux, which will scale with Ly$\alpha$ flux, in order to isolate the effects of the Ly$\alpha$ line which dominates the total UV flux.

### 2.2 Atmospheric modeling

GJ 436b is a mini-Neptune with 0.078 $M_{\rm Jupiter}$ and 0.369 $R_{\rm Jupiter}$, orbiting its host star at 0.03 AU (von Braun et al. 2012). We use a 1D model to calculate GJ 436b's atmospheric thermal structure and disequilibrium chemistry including molecular diffusion, vertical mixing and photochemistry (Miguel & Kaltenegger 2014).

We updated and improved the resolution of the cross sections for the different molecules in the FUV compared to previous studies (Kopparapu et al. 2012; Miguel & Kaltenegger 2014). Our new cross-section database includes high spectral-resolution measurements of absorption cross sections of high temperature $CO_2$ (Venot et al. 2013), $O_2$, $CH_4$ and $H_2O$ from the MPI-Mainz–UV-VIS Spectral Atlas of Gaseous Molecules [2], giving preference to the higher spectral-resolution measurements data (see also Bétrémieux & Kaltenegger (2013)). Note that due to the lack of data at longer wavelengths, the $H_2O$ cross section was extrapolated between 1900 and 2400 Å (Kopparapu et al. 2012) (black dotted lines in Fig. 3).

The 1D atmospheric chemistry model (see Miguel & Kaltenegger (2014) and Kopparapu et al. (2012) for a detailed explanation) considers equilibrium chemistry for higher temperatures and pressures and chemical disequilibrium in the upper atmosphere where the densities are low, and these processes have shorter timescales. The code includes disequilibrium processes (molecular diffusion, vertical mixing and photochemistry) and focuses on the following species in 179 reactions: O, O(1D), $O_2$, $H_2O$, H, OH, $CO_2$, CO, HCO, $H_2CO$, $CH_4$, $CH_3$, $CH_3O$, $CH_3OH$, CH, $CH_2$, $H_2COH$, C and $H_2$ (Kopparapu et al. 2012; Miguel & Kaltenegger 2014). Other important species like HCN and $C_2H_2$ are beyond the scope of this work and will be included in a future study. To characterize vertical-mixing processes in the atmosphere, we use a constant-eddy diffusion coefficient. Although this coefficient is difficult to constrain, results derived from comparisons between 1D and 3D models for HD 209458b show that the eddy-diffusion coefficient has values between $K_{ZZ} = 10^8$ and $K_{ZZ} = 10^{12}$ cm$^2$ s$^{-1}$ (Parmentier et al. 2013). Following these results, we adopt an intermediate value of $K_{ZZ} = 10^9$ cm$^2$ s$^{-1}$ in our calculations. Note that this value is not known for most hot extrasolar planets, and different values lead to differences in the upper atmosphere-mixing ratios (Visscher & Moses 2011; Miguel & Kaltenegger 2014). An exploration of extreme cases was performed by Miguel & Kaltenegger (2014) who showed that dissociation becomes less efficient as vertical mixing becomes stronger in the atmosphere which affects the atmospheric abundances and the effect of Ly$\alpha$ radiation in the atmosphere.

We obtained the temperature and pressure profiles from a radiative atmosphere model developed by for highly irradiated exoplanets by Guillot (2010) who found global mean thermal profiles comparable to detailed-atmospheric model calculations. The temperature structure of the exoplanet atmosphere as a function of the mean optical depth for thermal radiation ($\tau$) is given by equation (1) (Guillot 2010):

[1] http://cos.colorado.edu/kevinf/muscles.html

[2] www.uv-vis-spectral-atlas-mainz.org

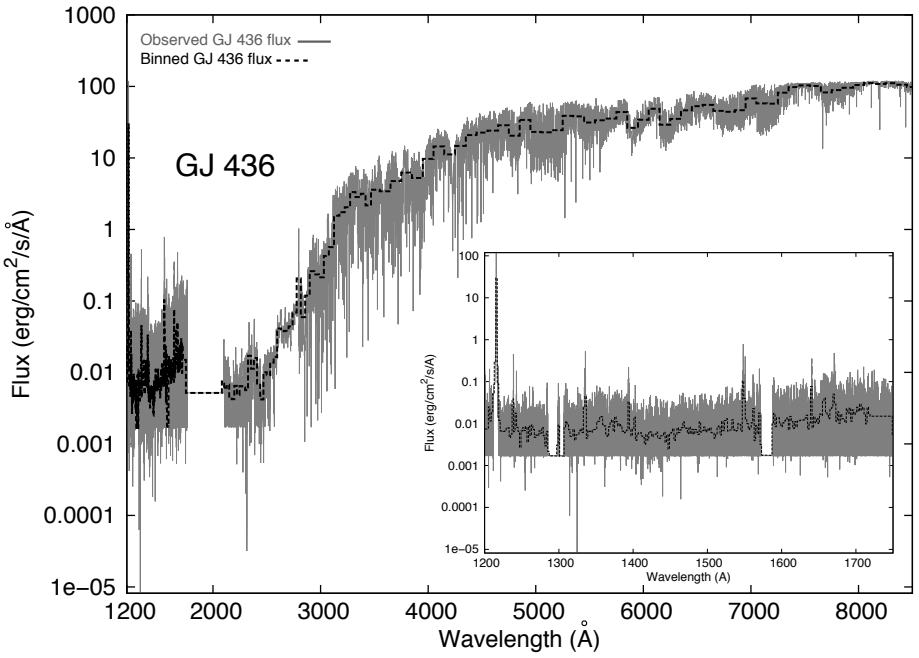


(a)

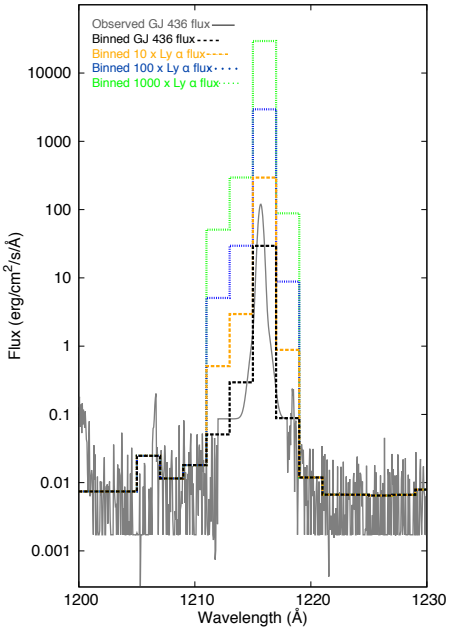


(b)

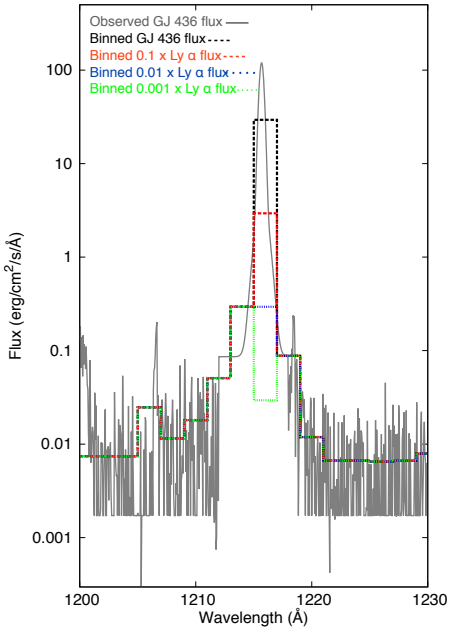


(c)

**Figure 1.** Flux of GJ 436 vs. wavelength obtained from UV direct measurements + model (grey), with the binning used in the code (black line). Flux between 1200 and 1800 Å is highlighted (right bottom panel). Figs. 1(b) and 1(c) show the different Lyα flux scenarios explored in the paper. Fig. 1(b): 1000 x Lyα (green dotted), 100 x Lyα (blue dotted) and 10 x Lyα (orange dots and dashes line). Fig. 1(c): 0.1 x Lyα (red dashed), 0.01 x Lyα (blue dotted) and 0.001 x Lyα (green dotted line). The flux values are normalized to 1AU.

$$T_p^4 = \frac{3T_{int}^4}{4}\left(\frac{2}{3}+\tau\right)+$$
$$\frac{3T_{irr}^4}{4} f\left(\frac{2}{3}+\frac{1}{\gamma\sqrt{3}}+\left(\frac{\gamma}{\sqrt{3}}-\frac{1}{\gamma\sqrt{3}}\right)e^{-\gamma\tau\sqrt{3}}\right). \quad (1)$$

We use $\gamma = 0.05$ which provides a good match to the thermal structures retrieved from observations of GJ 436b (Stevenson et al. 2010; Madhusudhan & Seager 2011; Moses et al. 2013) and GCMs models (Lewis et al. 2010). The planet's internal temperature ($T_{int}$) is usually adopted as 50 K for old mini-Neptunes [e.g. Miller-Ricci & Fortney (2010)], but GJ 436b has a high eccentricity [e=0.146 von Braun et al. (2012)] which implies a potentially tidally heated exoplanet (Agundez et al. 2014). We therefore adopt

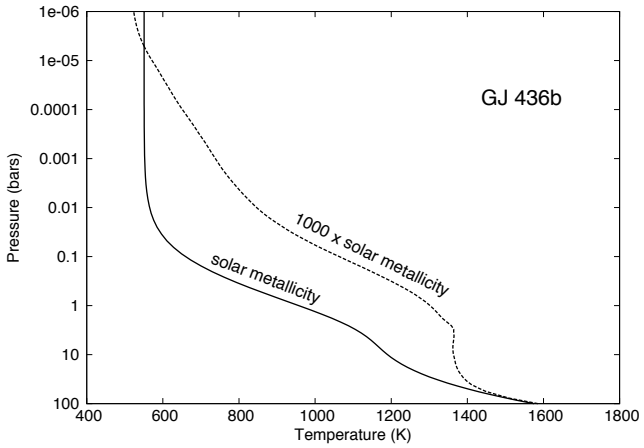


**Figure 2.** Temperature-pressure profile for GJ 436b for solar (solid) and 1000 x solar metallicity (dashed line) in the atmosphere.

$T_{int}$ = 300 K [following Guillot (2010)]. Different values of $T_{int}$ might change the thermal profile deep in the atmosphere (Moses et al. 2013; Agundez et al. 2014).

We use 100 atmospheric layers from $5\times10^{-8}$ to 200 bars. The thermal profile for GJ 436b is shown in Fig. 2 for solar metallicity (solid) and 1000 x solar enrichment (Moses et al. 2013) (dashed line). The 1000 x solar metallicity thermal profile was derived in Moses et al. (2013) using a PHOENIX model with the assumption that the stellar heating causes a circulation that inefficiently redistributes energy to the night side, as described in Barman et al. (2001, 2005).

## 3 RESULTS: EFFECT OF LY$\alpha$ FLUX ON MINI-NEPTUNE ATMOSPHERES

Photodissociation of atmospheric molecules occurs mostly in the upper atmosphere. This process is typically a one-way reaction which means that the probability of recombination and subsequent photon emission is negligible, thereby maintaining chemical disequilibrium in this region of the atmosphere.

All major species in mini-Neptune atmospheres considered in our model have a dissociation energy corresponding to wavelengths shorter than 2800 Å — $H_2O$ (dissociation energy 5.17 eV, equivalent to 2398 Å), $CO_2$ (5.52 eV or 2247 Å), $CH_4$ (4.55 eV or 2722 Å), $H_2$ (4.52 eV or 2743 Å) and CO (11.14 eV or 1113 Å). Therefore, UV radiation dominates the photochemistry in mini-Neptune atmospheres.

Fig. 3 shows the absorption cross sections as a function of wavelength for the most abundant molecules in the mini-Neptune atmospheres considered in this paper: $H_2$ (green) (Backx et al. 1976), $H_2O$ (black) (Mota et al. 2005), CO (brown) (Sun & Weissler 1955), $CH_4$ (blue) (Lee et al. 2001; Chen & Wu 2004) and $CO_2$ (red) (Huestis & Berkowitz 2010; Venot et al. 2013). Fig. 3(a) shows the region between 1200 and 2100 Å, and a larger region (between 200 and 2100 Å) is shown in Fig. 3(b).

Fig. 3 shows that $H_2O$ and $CH_4$ have higher cross sections between 1000 and 1400 Å and are especially susceptible to Ly$\alpha$ radiation from the host M star. Because of its short

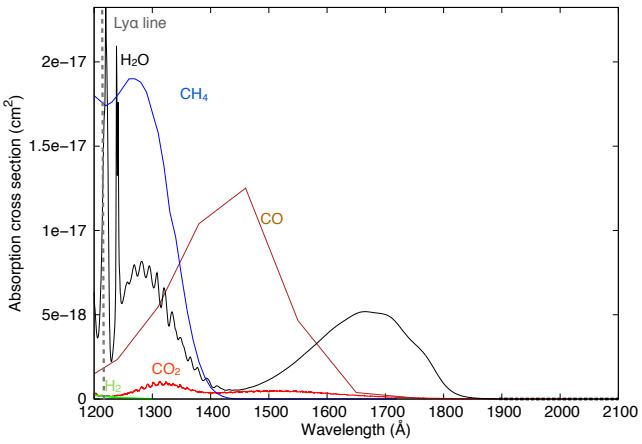


(a)

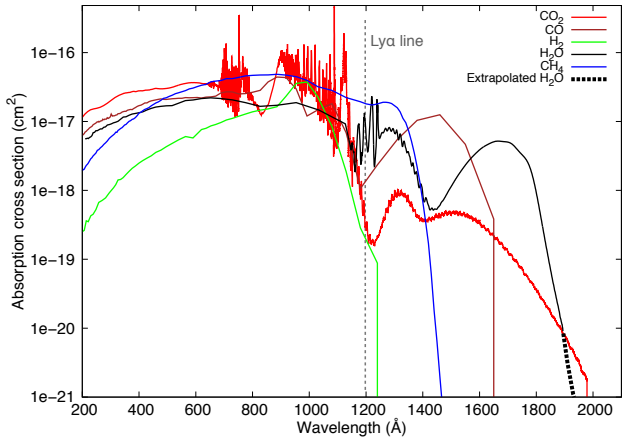


(b)

**Figure 3.** FUV cross sections vs. wavelength of some important molecules in GJ 436b's atmosphere: $H_2$ (green), $H_2O$ (black), $CH_4$ (blue), CO (brown) and $CO_2$ (red). Extrapolation of $H_2O$ cross section beyond 1900 Å is shown (black dotted line). The Ly$\alpha$ line is shown with grey-dashed line. The region between 1200 and 2100 Å is shown in Fig. 3(a), and between 200 and 2100 Å is shown in Fig. 3(b).

wavelength for dissociation, CO does not dissociate in response to FUV radiation, but has two peaks at 1332 and 1474 Å corresponding to the excitation of the various excited states of the molecule. As seen in the right top panel of Fig. 3, $CO_2$ is a strong absorber at short wavelengths ($\lambda < 1200$ Å, maximum at 900 Å), but $CO_2$ does not have a high cross section in the FUV. Even though $H_2$ has a small cross section in the FUV, it becomes a strong absorber at short wavelength ($\lambda < 1200$ Å) in exoplanet atmospheres because of its high abundance. Thus $H_2$ shields other molecules from very shortwave radiation.

EUV radiation is not included here because it is absorbed in the upper atmosphere and does not reach pressures in the range described in this paper. Note that the fate of Ly$\alpha$ photons as they travel through the extended H-rich thermosphere is not yet clear as this radiation could be significantly scattered by H in the planet's extended thermosphere (Lavvas et al. 2011; Koskinen et al. 2010) (see Section 3.2). A more detailed model of the extended upper at-

mosphere and atmospheric escape is beyond the scope of this paper.

Observations of GJ 436b's atmosphere indicate a CO-rich and $CH_4$-poor atmosphere (Stevenson et al. 2010; Madhusudhan & Seager 2011; Knutson et al. 2014). This composition can be explained by adopting high metallicities, between 230 to 2000 x solar (Moses et al. 2013). We therefore explore the effect of high FUV, and especially Ly$\alpha$, flux on mini-Neptune atmospheres, for solar (Section 3.1.1) as well as high metallicity (Section 3.1.2) atmospheric composition.

### 3.1 Effect of high Ly$\alpha$ flux

#### *3.1.1 Atmospheres with solar metallicities*

In Fig. 4(a), we show how the photolysis rates of the molecules most susceptible to dissociation by Ly$\alpha$ flux ($H_2O$, $CO_2$ and $CH_4$) change in the atmosphere for different irradiation scenarios: GJ 436b irradiated by 1000 x Ly$\alpha$, 100 x Ly$\alpha$, 10 x Ly$\alpha$, and 1 x Ly$\alpha$, where n x Ly$\alpha$ is the reconstructed Ly$\alpha$ flux for GJ 436b multiplied by the factor n [see Fig. 1(b)]. The photolysis rate of species $i$ ($r_i$) is proportional to the concentration of the species ($n_i$) and the photodissociation coefficient ($J_i$, shown in Fig. 4(b)) which depends only on the flux ($F$) and the cross section of the species ($\sigma_i$), as shown in equations (2) and (3) (Yung & Demore 1999):

$$r_i(z) = J_i(z)\ n_i(z), \tag{2}$$

$$J_i(z) = \int \sigma_i(\lambda)\ F(z,\lambda)\ d\lambda. \tag{3}$$

The $H_2O$ concentration is higher than $CH_4$ and $CO_2$ (see Fig. 5(a)) and, therefore, has higher photolysis rates. $H_2O$ absorbs most of the FUV radiation, becoming optically thick to radiation when $\lambda < 2000$ Å at $\sim 0.08$ bars. Lower photolysis rates at higher pressures are due to radiation at longer wavelengths ($2000 < \lambda < 2400$ Å).

Fig. 4(a) shows that high values of the Ly$\alpha$ flux (1000, 100, and 10 x Ly$\alpha$) lead to more radiation at higher pressures in the atmosphere, thereby increasing the $H_2O$, $CO_2$ and $CH_4$ photolysis rates.

Figs. 5(a) – 5(b) show mixing ratios vs. pressure of the most abundant species in GJ 436b's atmosphere with solar composition for four scenarios: 1000 x Ly$\alpha$ (small dotted), 100 x Ly$\alpha$ (dotted), 10 x Ly$\alpha$ (dots and dashes) and 1 x the reconstructed Ly$\alpha$ flux (solid line). For all species, mixing ratios in the four cases are the same for higher pressures, where photodissociation processes are not efficient, but start to deviate from equilibrium values when photodissociation of molecules occurs, mostly in the upper observable atmosphere ($P < 10^{-3}$bars).

Since GJ 436b is a cool planet with a $T_{eq} \sim 640$ K (assuming that the albedo=0), $CH_4$ is the most abundant carbon compound up to $10^{-4}$ bars for solar composition. At lower pressures, it is oxidized, and its abundance decreases rapidly. The $CH_4$ photolysis rate changes significantly with increasing Ly$\alpha$ flux (see Fig. 4(a)), as shown by the difference between the two extreme Ly$\alpha$ fluxes (1000 and 1 x Ly$\alpha$) being two orders of magnitude at $5 \times 10^{-5}$ bars, leading to different mixing ratios at lower pressures.

$H_2O$, which is the most abundant gas after He and $H_2$, starts to dissociate at $10^{-4}$ bars for 1000 x Ly$\alpha$, at $5 \times 10^{-5}$ bars for 100 x Ly$\alpha$, at $10^{-5}$ bars for 10 x Ly$\alpha$ and at $5 \times 10^{-6}$bars for the reconstructed Ly$\alpha$ flux.

The photolysis of $H_2O$ affects the mixing ratios of other species in the atmosphere such as O, OH and H which increase with increasing $H_2O$ photolysis. $H_2O$ dissociation is followed by the destruction of $H_2$ because of a reaction with OH. As a consequence of these reactions, a large amount of H is created and $H_2$ is destroyed with increasing Ly$\alpha$ flux. H replaces $H_2$ as the most abundant gas in the atmosphere at pressures $P < 5 \times 10^{-5}$ bars in all cases. OH increases with the Ly$\alpha$ flux because of the $H_2O$ photolysis at $\sim 10^{-5}$ bars. Note that CO photolysis is not considered because its photolysis is driven by EUV radiation which is not included in the model. Atomic O is produced from $H_2O$ photolysis. At $10^{-5}$ bars, its mixing ratio is $10^{-4}$ for 1000 x Ly$\alpha$ and $10^{-10}$ for 1 x Ly$\alpha$ flux.

CO and $CO_2$ show different behaviors compared to their chemistry in hot Jupiters' atmospheres, because CO is the dominant carbon compound in hot exoplanet atmospheres, whereas $CH_4$ is dominant in cooler planets. Self-shielding by $CH_4$ and other effects lead to differences in the chemistry and pressure where self-shielding occurs (Line et al. 2011). The CO-mixing ratio increases because of photochemistry at $\sim 0.01$ bars, increasing up to 2 orders of magnitude at $\sim 10^{-5}$ bars. $CO_2$ is formed after $H_2O$ photolysis, with a local maximum at $\sim 10^{-4}$ bars for 1000 x Ly$\alpha$, at $5 \times 10^{-5}$ bars for 100 x Ly$\alpha$, at $8 \times 10^{-6}$ bars for 10 x Ly$\alpha$ and at $10^{-6}$ bars for 1 x Ly$\alpha$.

Our results for the dominant carbon and oxygen species in GJ 436b for 1 x Ly$\alpha$ flux are in good agreement with previous results by Line et al. (2011) and Moses et al. (2013), with small differences due to differences in the UV fluxes used, cross sections adopted, chemical schemes and thermal profiles.

#### *3.1.2 Atmospheres with high metallicities*

High metallicities are expected in some mini-Neptune atmospheres because of the enrichment inferred from interior modeling (Baraffe et al. 2008; Figueira et al. 2009; Nettelmann et al. 2010) and from population synthesis models (Fortney et al. 2013). As a test case, we compute simulations for the atmosphere of GJ 436b assuming 1000 x solar metallicity.

An atmosphere with 1000 x solar metallicity has lower hydrogen and helium and increased carbon and oxygen abundances (Moses et al. 2013). Fig. 4(c) shows the photolysis rates of $CH_4$ (blue), $H_2O$ (black) and $CO_2$ (red) with the reconstructed Ly$\alpha$ flux of GJ 436 for a solar metallicity atmosphere (solid lines) and an atmosphere with 1000 x solar metallicity (dotted lines). $H_2O$ shows the highest photolysis rates for both compositions. The $CO_2$ photolysis rate is smaller than $CH_4$ for solar composition, but it increases for the 1000 x solar model, becoming larger than $H_2O$ at $P < 1 \times 10^{-6}$ bars. $CH_4$ has very low photolysis rates, especially for the case of an enriched atmosphere because it is shielded by $H_2O$ and $CO_2$.

Figs. 5(c) – 5(d) show mixing ratios vs. pressure for $H_2O$, $CO_2$, $CH_4$ and for H, $H_2$, O, CO and OH, respectively, for an atmosphere of 1000 x solar metallicity and four scenarios: 1000 x Ly$\alpha$ (small dotted), 100 x Ly$\alpha$ (dot-

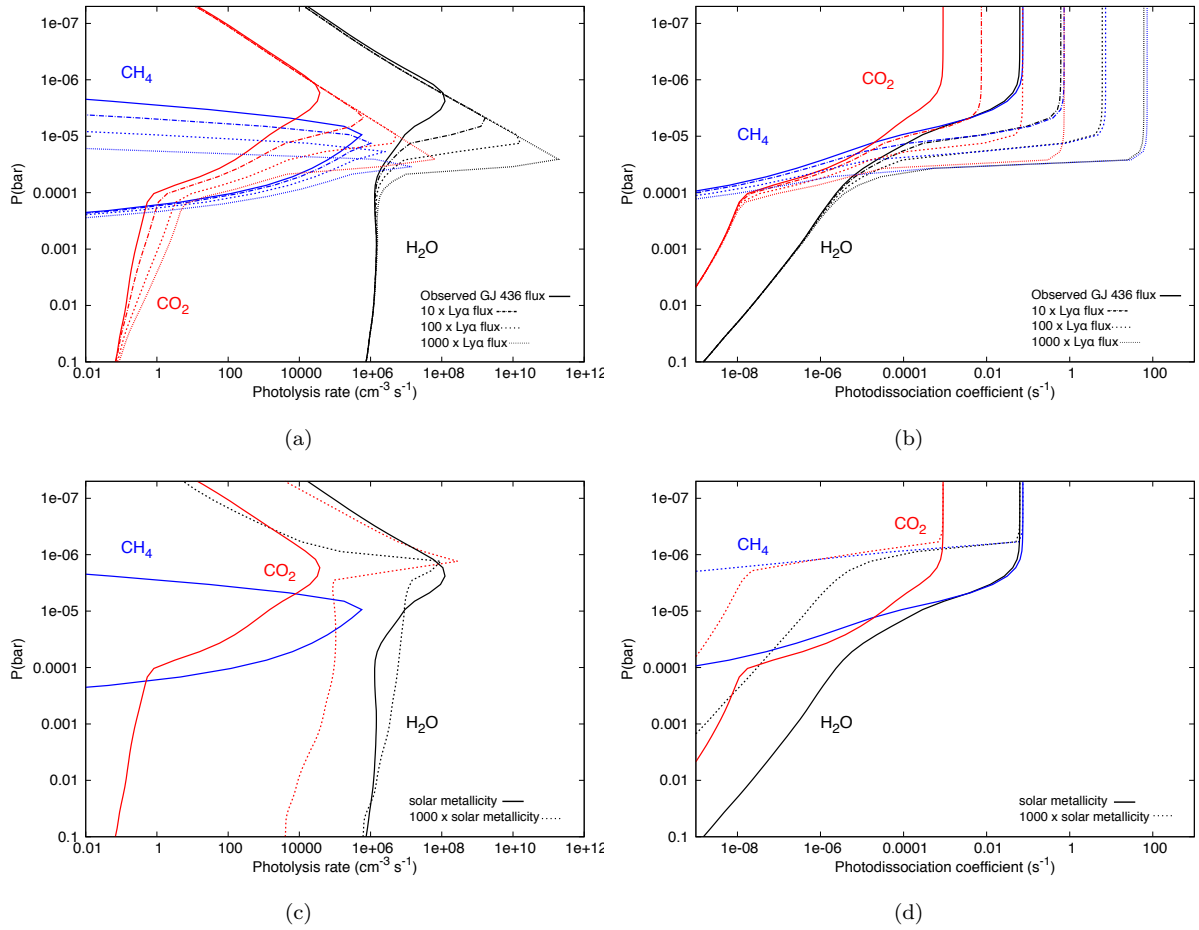


**Figure 4.** Photolysis rates (left panels) and photodissociation coefficient (right panels) vs. pressure in the atmosphere of GJ 436b for $H_2O$ (black), $CO_2$ (red) and $CH_4$ (blue). Top panels: *solar composition* for four Ly$\alpha$ flux scenarios: 1000 x Ly$\alpha$ (small dots), 100 x Ly$\alpha$ (dotted), 10 x Ly$\alpha$ (dots and dashes) and the reconstructed Ly$\alpha$ flux (solid line). Bottom panels: comparison between solar composition (solid) and 1000 x solar metallicity atmosphere (dotted lines) for the *reconstructed Ly$\alpha$ flux*. Note that solid lines in Figs. 4(c) – 4(d) are the same as in Fig. 4(a) – 4(b), respectively.

ted), 10 x Ly$\alpha$ (dots and dashes) and 1 x Ly$\alpha$ flux for GJ 436 (solid line). The photolysis rates (Fig. 4(c)) are reflected in the mixing-ratio profiles of $H_2O$, $CO_2$, $CH_4$ and those of the other molecules affected by $H_2O$ dissociation. Since $H_2O$ and $CO_2$ compete for photons, increased dissociation of $CO_2$ coincides with decreased dissociation of $H_2O$ compared to a solar metallicity atmosphere. As a consequence, H, $H_2$, O, CO and OH show less change for different irradiation cases. Dissociation of $H_2O$ and $CO_2$ starts at $5 \times 10^{-6}$ bars in all cases, but mixing ratios are smaller for larger Ly$\alpha$ fluxs. $CH_4$ shows very little change in the four scenarios because it is shielded by $H_2O$ and $CO_2$.

### 3.2 Absorption of Ly$\alpha$ radiation in the extended H atmosphere

Some hot extrasolar planets have an extended atmosphere consisting primarily of atomic H which could efficiently absorb Ly$\alpha$ radiation, as shown by observations (Vidal-Madjar et al. 2003; Lecavelier des Etangs et al. 2010; Ehrenreich et al. 2012) and theoretical models (Koskinen et al. 2010; Lavvas et al. 2011). Some absorption of Ly$\alpha$ photons has even been detected in GJ 436b's atmosphere (Kulow et al. 2014) which increases the importance of studying the absorption of Ly$\alpha$ radiation in an exoplanet's atmosphere and the effects on photochemistry. The exoplanet thermosphere is characterized by an increase in temperature (Huitson et al. 2012) which may affect the resulting atmospheric composition in the upper atmosphere ($P <\approx 10^{-7}$ bars) for some planets with extremely high temperatures. For those cases, thermochemical processes dominate the chemistry in the upper atmosphere, and the Ly$\alpha$ flux plays no role in defining the atmospheric composition (Lavvas et al. 2011). On the other hand, there are cooler planets, such as GJ 436b, for which the incident Ly$\alpha$ flux may be partially absorbed in the atmosphere, but the effects of this decreased flux on the resulting composition remain poorly understood. Lavvas et al. (2011) studied this problem and performed photochemical calculations taking into account the exoplanets' thermosphere for three planets, including GJ 436b, where they found that Ly$\alpha$ flux plays a small role in the photochemistry. In the present work, we use the FUV flux taken from recent observations (France et al. 2013) which is at least one order of magnitude larger than the FUV flux used in Lavvas et al. (2011). We assume that

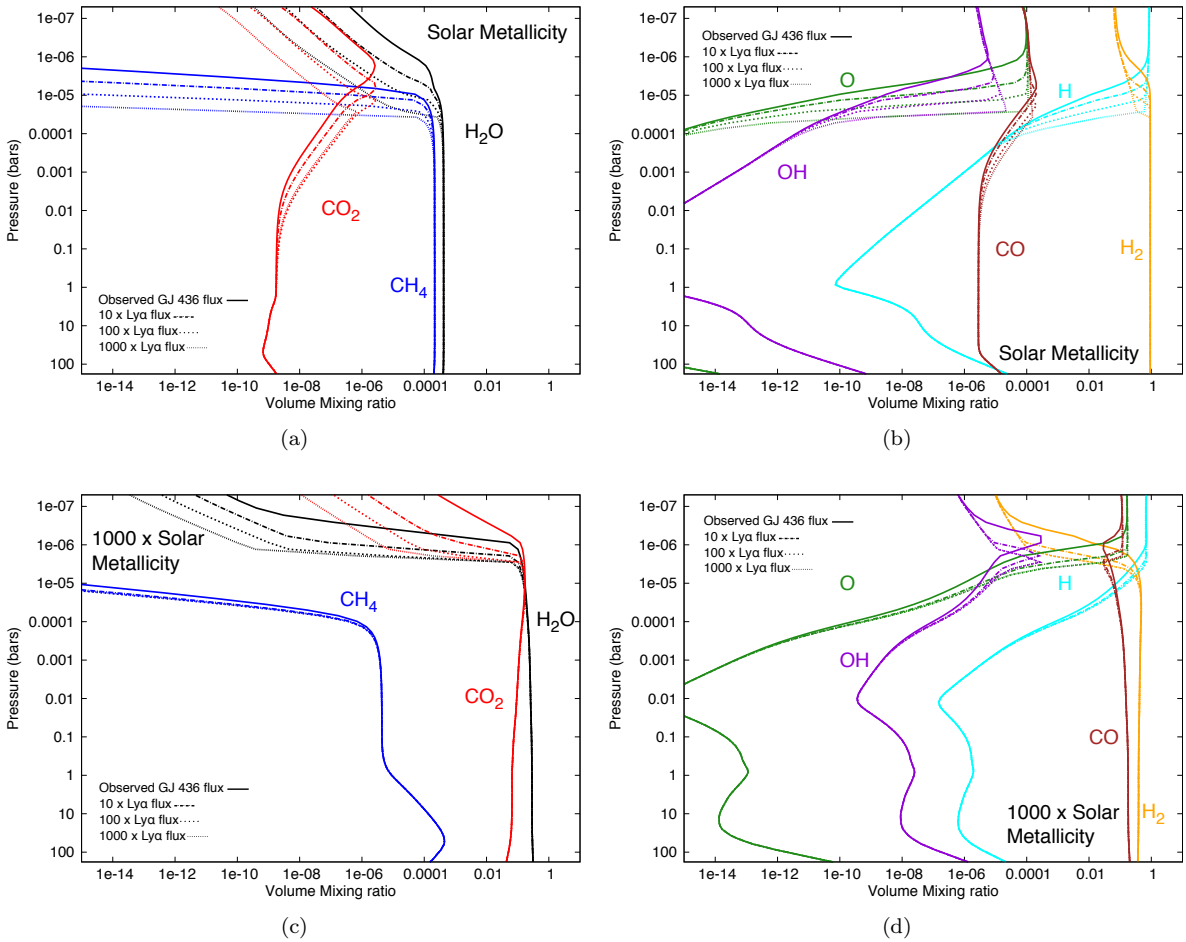


**Figure 5.** Mixing ratios vs. pressures for GJ 436b for solar (top panels) and 1000 x solar metallicity (bottom panels) atmospheres. Left panels (Figs. 5(a) and 5(c)) show gases affected by Ly$\alpha$ flux: $H_2O$ (black), $CH_4$ (blue), $CO_2$ (red) and their concentrations for different Ly$\alpha$ flux conditions: 1000 x Ly$\alpha$ flux (small dotted), 100 x Ly$\alpha$ (dotted), 10 x Ly$\alpha$ (dots and dashes) and 1 x the reconstructed Ly$\alpha$ flux (solid line). Right panels (Figs. 5(b) and 5(d)) show the H, $H_2$, O, CO and OH mixing ratios.

this Ly$\alpha$ radiation is not completely absorbed and therefore plays an important role in the photochemistry described in Section 3. It may be possible, nevertheless, that some Ly$\alpha$ radiation is absorbed. In this section, we explore the photochemistry effects of the absorption of Ly$\alpha$ flux in the atmosphere of GJ 436b. Since a self-consistent model of thermal structure, photochemistry and thermosphere is beyond the scope of this paper, we use a simplified model in which a portion of the stellar Ly$\alpha$ radiation is absorbed in the extended H atmosphere. We consider the three possible absorption scenarios shown in Fig. 1(c): 0.1 x Ly$\alpha$, 0.01 x Ly$\alpha$ and 0.001 x the reconstructed Ly$\alpha$ flux.

In Fig. 6 we show the mixing ratios of $H_2O$, $CH_4$, $CO_2$, O, OH, H, CO and $H_2$ as a function of the pressure in GJ 436b's atmosphere. We investigate the results of adopting solar composition (Fig. 6(a) – 6(b)) as well as 1000 x solar metallicity in the atmosphere (Fig. 6(c) – 6(d)) in the three explored scenarios (0.1 x Ly$\alpha$, 0.01 x Ly$\alpha$ and 0.001 x Ly$\alpha$). Since the atmosphere is exposed to reduced Ly$\alpha$ radiation, the photolysis rates are reduced in all cases compared to a deeper penetration of Ly$\alpha$ stellar flux (as adopted in Section 3). Decreased dissociation of $H_2O$ leads to an increase in its mixing ratio which is the highest in the case of extreme absorption (0.001 x Ly$\alpha$). For the case of solar composition, the mixing ratio of $H_2O$ at $5 \times 10^{-6}$ bars is $\sim 2 \times 10^{-6}$ for 1 x Ly$\alpha$ and $\sim 2 \times 10^{-4}$ for 0.001 x Ly$\alpha$ (Fig. 6(a)), and for 1000 x solar composition, it is $\sim 1 \times 10^{-7}$ for 1 x Ly$\alpha$ and 0.05 for 0.001 x Ly$\alpha$ at the same pressure (Fig. 6(c)). These changes in the $H_2O$-mixing ratios lead to changes in O, OH, H, CO and $H_2$ (see Fig. 6(b) – 6(d)).

For a solar composition atmosphere, the increase in the $CO_2$-mixing ratio at $\sim 1 \times 10^{-5}$ bars is a consequence of $H_2O$ photolysis, but the $CO_2$-mixing ratio decreases when there is less $H_2O$ dissociation for higher absorption of Ly$\alpha$ flux. The change between the extreme cases (1 x Ly$\alpha$ and 0.001 x Ly$\alpha$ flux) is one order of magnitude at $5 \times 10^{-6}$ bars. For solar composition and 1000 x solar metallicity atmospheres, the $CO_2$-mixing ratio at lower pressures ($P < 5 \times 10^{-6}$ bars) is dominated by its own dissociation, therefore the $CO_2$-mixing ratio increases for higher Ly$\alpha$ flux absorption. The difference in the $CO_2$-mixing ratios for the extreme cases (1 x Ly$\alpha$ and 0.001 x Ly$\alpha$) at $\sim 1 \times 10^{-7}$ bars is one order of magnitude for a solar metallicity atmosphere and two orders of magnitude for a 1000 x solar metallicity atmosphere.

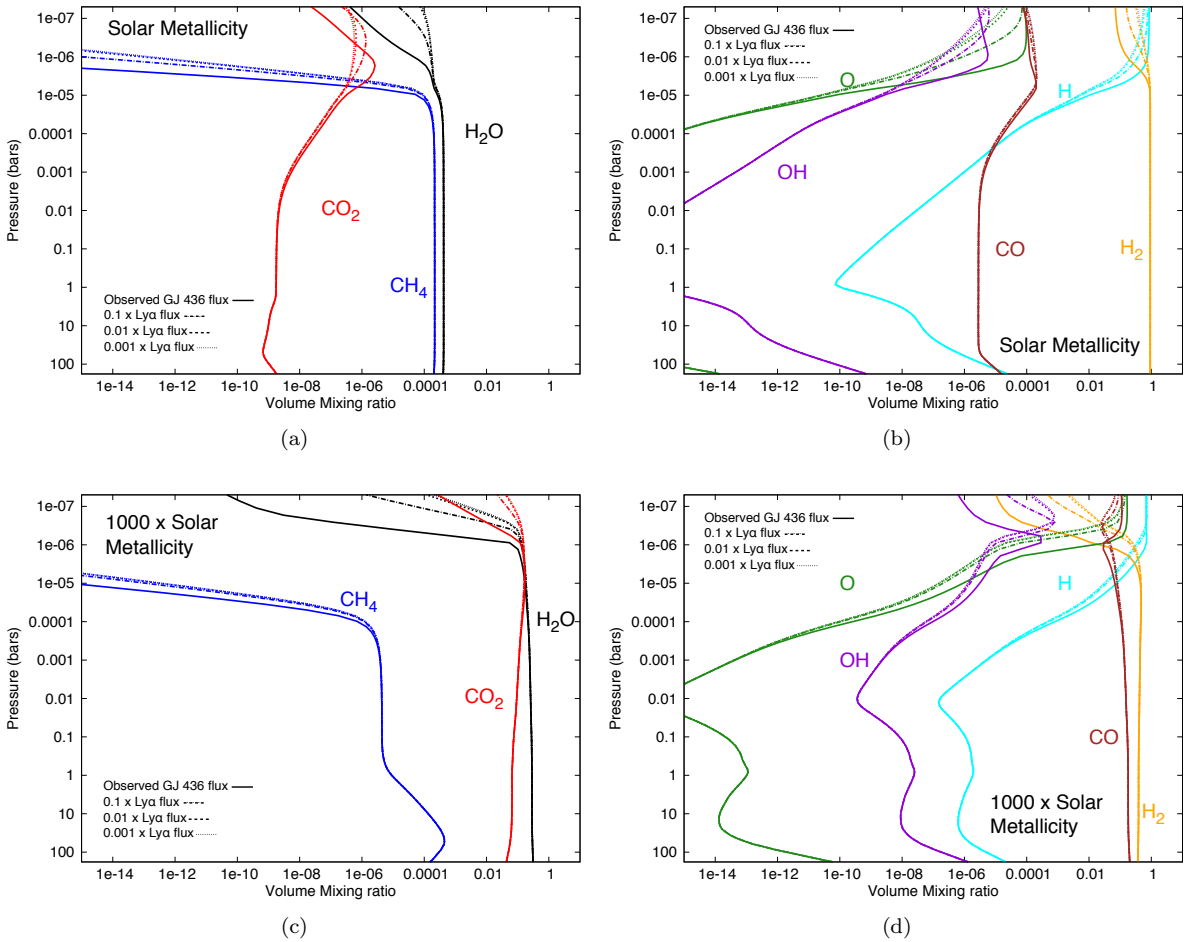


**Figure 6.** Photochemical mixing ratios vs. pressure for an atmosphere with solar composition (upper panels) and 1000 x solar metallicity (lower panels) for different Ly$\alpha$ absorption scenarios: 1 x Ly$\alpha$ (solid), 0.1 x Ly$\alpha$ (dots and dashes), 0.01 x Ly$\alpha$ (dashed) and 0.001 x Ly$\alpha$ flux (dotted line).

$CH_4$ dissociation is caused mainly by radiation around 1300 Å (see Fig. 3). Since this molecule is also shielded by $H_2O$ (solar composition) as well as by $H_2O$ and $CO_2$ (1000 x solar metallicity), its mixing ratio does not change significantly with increasing absorption of Ly$\alpha$ flux.

The absorption of Ly$\alpha$ radiation is important for the photochemistry in these exoplanet atmospheres. Different absorption scenarios lead to different mixing ratios and, therefore, it is necessary to know the amount of flux absorbed to know the effect on the photochemistry. Nevertheless, we notice that very strong absorption (0.001 x Ly$\alpha$ flux) has only a small effect on the photochemistry (compared to the case of 0.01 x Ly$\alpha$ flux) because the dissociation of molecules is mainly due to radiation at other wavelengths.

## 4 CONCLUSION

Ly$\alpha$ radiation changes mini-Neptunes' upper atmospheric chemistry significantly. We explore the effect of Ly$\alpha$-driven photochemistry for atmospheres with different metallicities, comparing solar composition and a 1000 x solar composition. Focusing on GJ 436b as an example, we calculate the thermal structure and chemistry including equilibrium and disequilibrium chemistry (molecular diffusion, vertical mixing, and photochemistry). We use direct observations of the UV and the reconstructed Ly$\alpha$ flux for the host star GJ 436 (France et al. 2013). We explore the effects on the planet's atmosphere of increasing the incident Ly$\alpha$ flux by factors of 10, 100 and 1000 as well as the case where the Ly$\alpha$ flux is absorbed in the extended H atmosphere by factors of 0.1, 0.01 and 0.001.

For solar composition atmospheres, our results show that the mixing ration of $H_2O$ is most affected by Ly$\alpha$ radiation as the $H_2O$ photolysis rate strongly depends on the Ly$\alpha$ flux even at pressures as large as $\sim$ 0.08 bars. The $H_2O$-mixing ratios change by up to five orders of magnitude between the cases of 1000 x Ly$\alpha$ and 0.001 x Ly$\alpha$. The reconstructed Ly$\alpha$ flux thereby significantly changes the upper atmospheric chemistry and the resulting observable spectral features. $H_2O$ is one of the most abundant gases in the atmosphere, absorbing much of the Ly$\alpha$ flux and shielding other species like $CH_4$. Changes in the $H_2O$ photolysis rates also affect other molecules whose mixing ratios are largely affected by $H_2O$ dissociation: for example, $CO_2$ changes by up to 3 orders of magnitude, OH by up to 5 orders of mag-

nitude, H by up to 4 orders of magnitude, O by up to 6 orders of magnitude, $H_2$ by 1 order of magnitude, and CO by less than 1 order of magnitude between the extreme cases of 1000 x Ly$\alpha$ and 0.001 x Ly$\alpha$ flux.

Because of the high abundance of $CO_2$ in high metallicity atmospheres, $CO_2$ competes with $H_2O$ for energetic FUV photons. The $CO_2$ photolysis rate is largely affected by the Ly$\alpha$ flux, and therefore its mixing ratio changes by up to 4 orders of magnitude for the extreme irradiation scenarios we have explored. These two molecules absorb most of the Ly$\alpha$ radiation, thereby shielding $CH_4$. The smaller effect on $H_2O$ also leads to smaller changes in the abundance of those other molecules for which mixing ratios in the upper atmosphere strongly depend on $H_2O$ photolysis.

Our models show that Ly$\alpha$ radiation from the host star affects mini-Neptune atmospheres significantly at low pressures and cannot be ignored in atmospheric modeling. Ly$\alpha$ radiation affects the photochemistry of important gases in the upper atmosphere and, therefore, also the resulting observable spectral features of mini-Neptunes. Observations of the UV flux from a wide range of stars as well as studies of the absorption of this radiation in the exoplanet thermospheres are essential for realistic interpretations of planetary spectra.

## ACKNOWLEDGEMENTS

We would like to thank Ravi Kopparapu, James Kasting, Dimitar Sasselov, Kevin France and Yan Betremieux for useful discussions. Special thanks to Julianne Moses, for fruitful discussions and providing the thermal structure of high-metallicity GJ 436b atmosphere. YM and LK acknowledge DFG funding ENP Ka 3142/1-1 and the Simons Foundation. JLL acknowledges support from the Space Telescope Science Institute. This work has made use of the MUSCLES M dwarf UV radiation field database.

## REFERENCES

Agúndez, M., Venot, O., Selsis, F., Iro, N., 2014, ApJ, 781, 68
Allard, F., Hauschildt, P. H., Alexander, D. R., Tamanai, A., Schweitzer, A., 2001, ApJ, 556, 357
Allard, F., Allard, N. F., Homeier, D., Kielkopf, J., McCaughrean, M. J., Spiegelman, F., 2007, A&A 474, L21
Au, J.W., Cooper, G., Burton, G.R., Olney, T.N., Brion, C.E., 1993, Chem. Phys., 173, 209
Backx, C., Wight, G.R., Van der Wiel, M.J., 1976, J. Phys. B: Atom. Mol. Phys., 9, 315
Baraffe, I., Chabrier, G., Barman, T., 2008, A&A, 482, 315
Barman, T. S., Hauschildt, P. H., Allard, F., 2001, ApJ, 556, 885
Barman, T. S., Hauschildt, P. H., Allard, F., 2005, ApJ, 632, 1132
Bétrémieux, Y., Kaltenegger, L., 2013, ApJL, 772, L31
Bonfils, X. et al., 2012, A&A, 546, A27
Borucki, W. J. et al., 2011, ApJL, 736, 19
Buccino, A. P., Lemarchand, G. A., Mauas, P. J. D., 2007, Icarus, 192, 582
Butler, R. P. et al., 2004, ApJ, 617, 580
Chabrier, G., 2003, PASP, 115, 763
Charbonneau, D. et al., 2009, Nature, 462, 891
Chen, F. Z., Wu, C. Y. R., 2004, JQSRT, 85, 195
Ehrenreich, D., Lecavelier Des Etangs, A., Delfosse, X., 2011, A&A, 529, A80
Ehrenreich, D. et al., 2012, A&A, 547, A18
Figueira, P. et al., 2009, A&A, 493, 671
Fortney, J. J. et al., 2013, ApJ, 775, 80
France, K. et al., 2013, ApJ, 763, 149
Guillot T., 2010, A&A, 520, A27
Huestis, D. L., Berkowitz, J., 2010, AdG, 25, 229
Huitson, C. M. et al., 2012, MNRAS, 422, 2477
Knutson, H. A., Benneke, B., Deming, D., Homeier, D., 2014, Nature, 505, 66
Kopparapu, R. K., Kasting, J. F., Zahnle, K. J., 2012, ApJ, 745, 77
Koskinen, T. T., Yelle, R. V., Lavvas, P., Lewis, N. K., 2010, ApJ, 723, 116
Kulow, J., R., France, K., Linsky, J., Parke Loyd, R. O., 2014, ApJ, 786, 132
Kroupa, P., 2002, Science 295, 82
Lammer, H. et al., 2003, ApJL, 598, L121
Lammer, H. et al., 2011, Ap&SS, 335, 39
Lavvas, P., Koskinen, T., Yelle, R. V., 2011, EPSC-DPS Joint Meeting 2011, 645
Laughlin, G., Bodenheimer, P., Adams, F. C., 2004, ApJL, 612, L73
Lecavelier des Etangs, A., Vidal-Madjar, A., McConnell, J. C., Hébrard, G., 2004, A&A, 418, L1
Lecavelier Des Etangs, A. et al., 2010, A&A, 514, A72
Lecavelier des Etangs, A. et al., 2012, A&A, 543, L4
Lee, A. Y. T. et al., 2001, ApJL, 551, L93
Lewis, N. K., Showman, A. P., Fortney, J. J., Marley, M. S., Freedman, R. S., Lodders, K., 2010, ApJ, 720, 344
Linsky, J. L., France, K., Ayres, T., 2013, ApJ, 766, 69
Line, M. R., Vasisht, G., Chen, P., Angerhausen, D., Yung, Y. L., 2011, ApJ, 738, 32
Madhusudhan, N., Seager, S., 2011, ApJ, 729, 41
Maness, H. L. et al., 2007, PASP, 119, 90
Marcy, G. W., Chen, G. H. 1992, ApJ, 390, 550
Miguel, Y., Kaltenegger L., 2014, ApJ, 780, 166
Miller-Ricci, E., Fortney, J. J., 2010, ApJ, 716, 74
Mota, R. et al., 2005, Chem. Phys. Lett., 416, 152
Moses, J. I. et al., 2011, ApJ, 737, 15
Moses, J. I. et al., 2013, preprint (arXiv:1306.5178)
Murray-Clay, R. A., Chiang, E. I., Murray, N., 2009, ApJ, 693, 23
Nettelmann, N., Kramm, U., Redmer, R., Neuhäuser, R., 2010, A&A, 523, A26
Parmentier, V., Showman A., Lian Y., 2013, A&A, 558, A91
Poppenhaeger, K., Robrade, J., Schmitt, J. H. M. M., 2010, A&A, 515, A98
Rojas-Ayala, B., Covey, K. R., Muirhead, P. S., Lloyd, J. P., 2012, ApJ, 748, 93
Rugheimer, S. et al., 2014, in preparation
Sanz-Forcada, J. et al., 2011, A&A, 532, A6
Scalo, J. et al., 2007, Astrobiology, 7, 85
Segura, A., Walkowicz, L M., Meadows, V., Kasting, J., Hawley, S., 2010, Astrobiology, 10, 751
Shkolnik, E. L., & Barman, T. S. 2014, AJ, 148, 64
Stevenson, K. B. et al., 2010, Nature, 464, 1161
Sun, H., Weissler,G. L., 1955, J. Chem. Phys., 23, 1625

Tan, K.H, Brion, C.E., van der Leeuw, P.E. , van der Wiel, M.J., 1978, Chem. Phys., 29, 299
Venot, O. et al., 2013, A&A, 551, A131
Vidal-Madjar, A. et al., 2003, Nature, 422, 143
Visscher, C., Moses, J. I., 2011, ApJ, 738, 72
von Braun, K. et al., 2012, ApJ, 753, 171
Yelle, R. V., 2004, Icarus, 170, 167
Yelle, R. V., 2006, Icarus, 183, 508
Yung, Y. L., Demore, W. B., 1999, Photochemistry of planetary atmospheres, Oxford University Press: New York